The Transient Accumulation of the Signaling State of Photoactive Yellow Protein Is Controlled by the External pH

Berthold Borucki,* Chandra P. Joshi,* Harald Otto,* Michael A. Cusanovich,† and Maarten P. Heyn*

*Biophysics Group, Department of Physics, Freie Universität Berlin, 14195 Berlin, Germany; and †Department of Biochemistry and Molecular Biophysics, University of Arizona, Tucson, Arizona, 85721

ABSTRACT The signaling state of the photoreceptor photoactive yellow protein is the long-lived intermediate I_2'. The pH dependence of the equilibrium between the transient photocycle intermediates I_2 and I_2' was investigated. The formation of I_2' from I_2 is accompanied by a major conformational change. The kinetics and intermediates of the photocycle and of the photoreversal were measured by transient absorption spectroscopy from pH 4.6 to 8.4. Singular value decomposition (SVD) analysis of the data at pH 7 showed the presence of three spectrally distinguishable species: I_1, I_2, and I_2'. Their spectra were determined using the extrapolated difference method. I_2 and I_2' have electronic absorption spectra, with maxima at 370 ± 5 and 350 ± 5 nm, respectively. Formation of the signaling state is thus associated with a change in the environment of the protonated chromophore. The time courses of the I_1, I_2, and I_2' intermediates were determined from the wavelength-dependent transient absorbance changes at each pH, assuming that their spectra are pH-independent. After the formation of I_2' (~2 ms), these three intermediates are in equilibrium and decay together to the initial dark state. The equilibrium between I_2 and I_2' is pH dependent with a pK_a of 6.4 and with I_2' the main species above this pK_a. Measurements of the pH dependence of the photoreversal kinetics with a second flash of 355 nm at a delay of 20 ms confirm this pK_a value. I_2 and I_2' are photoreversed with reversal times of ~55 μs and several hundred microseconds, respectively. The corresponding signal amplitudes are pH dependent with a pK_a of ~6.1. Photoreversal from I_2' dominates above the pK_a. The transient accumulation of I_2', the active state of photoactive yellow protein, is thus controlled by the proton concentration. The rate constant k_3 for the recovery to the initial dark state also has a pK_a of ~6.3. This equality of the equilibrium and kinetic pK_a values is not accidental and suggests that k_3 is proportional to $[I_2']$.

INTRODUCTION

Photoactive yellow protein (PYP) is significant as the structural prototype for a large and diverse superfamily of signaling proteins that share a common structural motif termed the PAS domain (1,2). PAS domains are found in all kingdoms of life, generally as the sensory component of multi-domain proteins. The structure of PYP has a central six-stranded antiparallel β-sheet, with four structural features: an N-terminal cap, a PAS core with the first three β-strands of the central β-sheet, a helical connector, and a so-called β-scaffold consisting of the last three β-strands (3–7). PYP from the halophilic purple phototrophic bacterium *Halorhodospira halophila* is a small 14-kDa soluble cytoplasmic protein. The physiological function of *H. halophila* PYP was reported to be in negative phototaxis, resulting in movement away from blue/UV light (8). Its chromophore is *p*-hydroxycinnamic acid covalently bound via a thioester linkage to cysteine-69. In the dark, the phenol group of the chromophore is deprotonated, and the $C_7{=}C_8$ bond is *trans*. The ionization of the chromophore and its hydrogen bonding to E-46 and Y-42 are mainly responsible for the observed spectral tuning in the dark state ($\lambda_{max} \approx 446$ nm). Light-induced *trans–cis* isomerization around the $C_7{=}C_8$ bond is rapid (<3 ps) and is followed by a sequence of slower relaxations in the dark that ultimately lead to recovery of the dark state in less than 1 s. This photocycle has already been studied in considerable detail (9–11). The first long-lived intermediate, after the two very short-lived intermediates I_0 and $I_0^{\ddagger}$, is I_1. I_1 forms in ~3 ns and has a red-shifted absorption spectrum ($\lambda_{max} \approx 460$ nm). In several hundred microseconds it decays to I_2. I_2 has a protonated chromophore and a blue-shifted absorption spectrum that is commonly believed to have its λ_{max} value at 355 nm. In I_2 the chromophore phenol is partially exposed to the aqueous medium and hydrogen-bonded to the side chain of R-52 (6). The protonation of the chromophore occurs either intramolecularly from E-46 (12) or from the external medium (13). In several milliseconds I_2 is transformed into I_2'. I_2' is believed to be the signaling state. It also has a protonated chromophore with a λ_{max} value similar to that of I_2. The I_2 to I_2' transition is associated with a major global structural change, which has been documented by NMR (14,15), CD (16), small-angle x-ray scattering (17), and FTIR (12,18). Formation of I_2' is associated with exposure of a hydrophobic surface patch (19), presumably the recognition and binding site for a response regulator. Experiments with hydrophobic dyes showed that these bind transiently to I_2' but not to I_2 (13). PYP shares a number of features, such as spectral tuning, photoisomerization, transient chromophore (de)protonation, and photoreversal, with other photoreceptors such as rhodopsin and phytochrome. This together with the availability

Submitted April 10, 2006, and accepted for publication June 15, 2006.

Address reprint requests to Maarten P. Heyn, Biophysics Group, Dept. of Physics, Freie Universität Berlin, Arnimallee 14, 14195 Berlin, Germany. Tel: 49-30-83856160; Fax: 49-30-83856299; E-mail: heyn@physik.fu-berlin.de.

0006-3495/06/10/2991/11 $2.00

doi: 10.1529/biophysj.106.086645

of high-resolution structures of intermediates (3–7) makes PYP an attractive model system for signal transduction (1).

For an understanding of the mechanism of PYP, a detailed characterization of its photocycle is essential. Such studies have been carried out by both electronic (9–11,20) and vibrational (21,22) spectroscopy. The photocycle kinetics are pH (23–25) and salt (26,27) dependent. Whereas early models assumed a unidirectional sequential mechanism (9,20), it is becoming increasingly clear that back reactions and equilibria between intermediates play essential roles (11,24,25,28). These equilibria are also pH (24–26,28–30) and salt dependent (26). An example of the pH- and salt-dependent equilibrium between I_1 and I_2/I_2' was recently described for the mutant Y98Q (26). At alkaline pH, the $I_1'$and I_2' intermediates are in equilibrium with a pK_a of ~9.9 (25,28). Most photocycle intermediates can be photoreversed when excited with light of the appropriate wavelength at the right time (31–33). Using this double-flash method, we showed that the I_2 and I_2' intermediates are in equilibrium (33). I_2 partly decays to I_2' in ~2 ms and then remains in equilibrium with I_2' until the end of the cycle (33). Our laboratory showed from time-resolved fluorescence and photostationary absorption measurements that this I_2/I_2' equilibrium is pH dependent with a pK_a of 6.3 (34). Interestingly the rate constant for the kinetics of the ground state recovery has a bell-shaped pH dependence with a lower pK_a of 6.4 (23), i.e., identical to the value for the I_2/I_2' equilibrium (34). The nature of the group(s) responsible for this pK_a is still not entirely certain, but it is commonly ascribed to E-46 (35,36).

The I_2 and I_2' intermediates were originally characterized by time-resolved FTIR spectroscopy (12,18), but they can also be distinguished by transient absorption spectroscopy in the UV/visible. Indeed, our laboratory recently obtained λ_{max} values of 372 and 352 nm for I_2 and I_2', respectively, from measurements of the pH dependence of the photostationary absorbance in the presence of background illumination (34). Here we characterize the equilibrium and spectra of the I_2 and I_2' intermediates by kinetic methods using transient absorption spectroscopy in the UV/visible and the extrapolated difference method (37). These methods allow a direct determination of the time-dependent intermediate populations and their pH dependencies. We find that the transient accumulation of the signaling state (I_2') increases with pH with a pK_a of ~6.4.

MATERIALS AND METHODS

Protein production and purification

H. halophila holo-PYP was produced by coexpression with the biosynthetic enzymes TAL and pCL and subsequently purified from *Escherichia coli* BL 21 (DE3) as described (38).

Transient absorption spectroscopy

Time-resolved absorption spectroscopy with single- and double-flash excitation was performed as described (13,24,33,39). To resolve the photoreversal kinetics, the data acquisition was triggered on the second flash (33,39). SVD methods were used as described (13,24,40–42).

Data analysis

Spectra and time courses of intermediates were obtained using the extrapolated difference method as described (25,37). The transient absorbance change $\Delta A(\lambda, t)$ is given by a sum of contributions from the spectral intermediates i, whose relative concentration is given by $n_i(t)$. In matrix notation:

$$\Delta\mathbf{A} = (\mathbf{A} - \mathbf{A}_p)\mathbf{n} \quad (1)$$

where the columns of $\mathbf{A}$ are the spectra of intermediates and each of the identical columns of $\mathbf{A}_p$ is the spectrum of the dark state P. Assuming first-order kinetics, $\Delta\mathbf{A}$ can be represented by a sum of exponentials. The wavelength-dependent coefficients of the exponentials are the amplitude spectra $B_i(\lambda)$. The $B_i(\lambda)$ are given in matrix notation by:

$$\mathbf{B} = (\mathbf{A} - \mathbf{A}_p)\mathbf{C} \quad (2)$$

where C_{ij} is the weight of the jth exponential in the time dependence of $n_i(t)$.

The amplitude spectra are ordered from low to high apparent time constants in the matrix $\mathbf{B}$. New matrices $\tilde{\mathbf{B}}$ and $\tilde{\mathbf{C}}$ are formed from the columns of $\mathbf{B}$ and $\mathbf{C}$ by adding up columns (25,37). The columns of $\tilde{\mathbf{B}}$ represent the extrapolated absorption difference spectra; the columns of $\tilde{\mathbf{C}}$ contain the relative contributions of the intermediates in these difference spectra. In the case of PYP at acid and neutral pH, only three intermediates contribute, as we will see, in the time range investigated: I_1, I_2, and I_2'. Their relative contributions to the ith extrapolated absorption difference spectrum will be called (x_i, y_i, z_i) in the order I_1, I_2, I_2'.

The intermediate spectrum $(\mathbf{A})_i$ can then be calculated from column i of matrix $\tilde{\mathbf{C}}^{-1}$:

$$(\mathbf{A})_i = \tilde{\mathbf{B}}(\tilde{\mathbf{C}}^{-1})_i + (\mathbf{A}_p)_i \quad (3)$$

To calculate the elements of $\tilde{\mathbf{C}}$ the following two constraints are introduced:

1. The sum of the relative intermediate concentrations of I_1, I_2, and I_2' in the extrapolated difference spectra is constant at all times before ground state recovery and equals the fraction of molecules cycling, η. This means that the sum of x, y, and z for each extrapolated difference spectrum equals η or that the sum of the matrix elements of each column of $\tilde{\mathbf{C}}$ equals η, and that of $\tilde{\mathbf{C}}^{-1}$ is $1/\eta$. This is simply the conservation law for the number of cycling molecules in a sequential cycle.
2. The absorption of I_2' is identical to zero for wavelengths larger than or equal to 410 nm. I_2' has its absorption maximum for the longest wavelength S_0-S_1 transition around 355 nm. Because the spectra of all intermediates have similar bandwidths, we can estimate from the spectrum of P, which does not absorb beyond 500 nm, that I_2' does not absorb beyond 410 nm.

Matrix calculations were performed with Matlab version R12.1. Fits with sum of exponentials were carried out with Microcal Origin 7.5.

RESULTS

Spectra and time courses of intermediates at pH 7: extrapolated difference method

Transient absorbance changes were measured at 19 wavelengths, ranging from 330 to 510 nm, in the time domain from 50 ns to 5 s. Fig. 1 *A* shows data at pH 7. For clarity, time traces at only eight wavelengths are shown. The complete data set was subjected to SVD analysis. The first

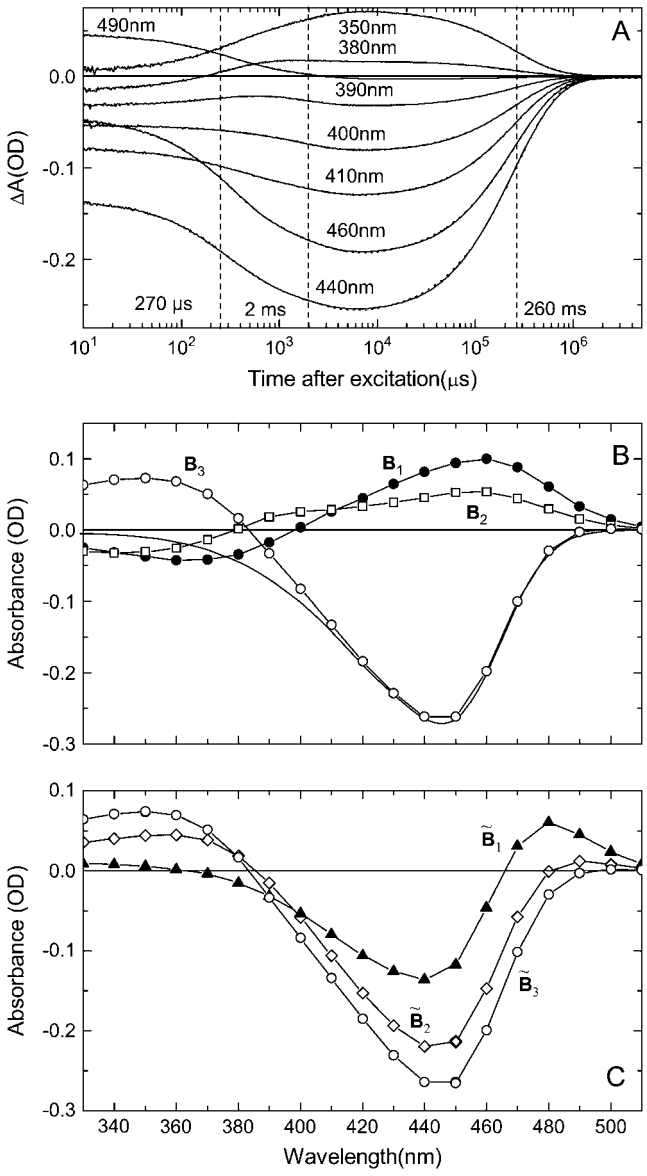

FIGURE 1 (*A*) Transient absorption changes after excitation at 430 nm at 19 wavelengths varying from 330 to 510 nm. For clarity, only the traces at the indicated wavelengths are shown. The vertical dashed lines indicate the time constants for a global fit to the weighted SVD time traces with a sum of three exponentials. $\tau_1 = 270\ \mu$s is the rise time of I_2, $\tau_2 = 2.0$ ms is the rise time of I_2', and $\tau_3 = 260$ ms is the return to P. The dotted lines, only distinguishable from the data in the microsecond time range, are the fits. Conditions: pH 7, 20°C, 50 mM KCl, and 50 mM Tris. PYP concentration 35 μM. (*B*) Amplitude spectra $B_i(\lambda)$ calculated from the amplitudes of the exponential fits to the SVD time traces and the corresponding basis spectra of the data in *A*. The three amplitude spectra correspond to the following time constants: $\tau_1 = 270\ \mu$s (●), $\tau_2 = 2.0$ ms (□), $\tau_3 = 260$ ms (○). The solid curve is a scaled and inverted ground-state spectrum. (*C*) Extrapolated difference spectra obtained from the amplitude spectra of *B* as described in the text: $\tilde{\mathbf{B}}_1$ (▲), $\tilde{\mathbf{B}}_2$ (◇), and $\tilde{\mathbf{B}}_3$ (○).

six singular values were 11.2, 1.8, 0.14, 0.05, 0.03, and 0.02. We consider the first three to be significant, suggesting the presence of only three spectrally distinguishable intermediates. The additional components (s_4, s_5, and s_6) show very noisy time traces and were therefore neglected. The three weighted time traces from SVD were fitted simultaneously starting at 10 μs with a sum of three exponentials with time constants $\tau_1 = 270\ \mu$s, $\tau_2 = 2.0$ ms, and $\tau_3 = 260$ ms. These times are marked by vertical dashed lines in Fig. 1 *A*. The dotted lines in Fig. 1 *A*, which can barely be distinguished from the data, represent these fit curves for the individual time traces. From the fit to the SVD time traces and the corresponding basis spectra, the amplitude spectra $B_j(\lambda)$ were calculated as described (42). These are presented in Fig. 1 *B*. The amplitude spectra provide considerable insight into the spectra of the intermediates. $B_1(\lambda)$ clearly describes the transition from I_1 ($\lambda_{max} \approx 460$ nm) to I_2 with a λ_{max} value above 360 nm. $B_2(\lambda)$ is apparently a transition from an equilibrium of I_1 and I_2 to I_2' with I_2' blue-shifted with respect to I_2. $B_3(\lambda)$ represents the ground state recovery and suggests that I_2' has its λ_{max} value near 350 nm. Comparison of the negative minimum of $\mathbf{B}_1$ with the positive maximum of $\mathbf{B}_3$ suggests that the transition from I_2 to I_2' is associated with a blue shift of the order of ~20 nm. So qualitatively the conclusion that there is a blue shift between the early UV intermediate I_2 and the later UV intermediate I_2' is already apparent from the data alone (amplitude spectra) without any model-dependent assumptions. The following quantitative analysis, which does use two plausible constraints, strengthens this conclusion.

We recently described in detail how to construct the intermediate spectra and time courses from the **B** spectra using the extrapolated difference method (25,37). The main equations were briefly summarized in Materials and Methods. The three amplitude spectra $\mathbf{B}_1$, $\mathbf{B}_2$, and $\mathbf{B}_3$ were used to construct the $\tilde{\mathbf{B}}$ matrix as described (25,37). The three columns, $\tilde{\mathbf{B}}_1$, $\tilde{\mathbf{B}}_2$, and $\tilde{\mathbf{B}}_3$, representing the extrapolated difference spectra are presented in Fig. 1 *C*. $\tilde{\mathbf{B}}_1$ equals the initial absorbance change right after the flash and suggests that the initial bleach led to the formation of the I_1 intermediate (positive absorbance change near 480 nm).

We now use the second constraint as described in Materials and Methods, that I_2' does not absorb beyond 410 nm, and consider Eq. 3 only in the range $\lambda > 410$ nm; i.e., we drop the rows for the shorter wavelengths. Then the third column of the reduced matrix **A**, corresponding to the spectrum of I_2', is the null vector: $(\mathbf{A})_3 = \vec{0}$. Because $(\mathbf{A})_3$ is zero, we can solve Eq. 3 for $(\tilde{\mathbf{C}}^{-1})_3$. In this way, we determine the third column of $\tilde{\mathbf{C}}^{-1}$. Under the first constraint, the sum of these matrix elements equals η^{-1}. In this way, we find, for the fraction of molecules cycling, $\eta = 0.371$. Finally, using $\tilde{\mathbf{B}}$ and $\mathbf{A}_p$ for the whole spectral range allows us to calculate the spectrum of I_2' from $(\tilde{\mathbf{C}}^{-1})_3$ using Eq. 3. The result is shown in Fig. 2 *A* (*solid squares*). The λ_{max} value of the spectrum is at ~350 ± 5 nm.

Because only I_1 contributes to $\tilde{\mathbf{B}}_1$ (see Fig. 1 *C*), the elements $\tilde{C}_{21} = y_1$ and $\tilde{C}_{31} = z_1$ of $\tilde{\mathbf{C}}$ are given by $y_1 = z_1 = 0$. This allows us to calculate the elements of the first column of $\tilde{\mathbf{C}}^{-1}$. The result is $\tilde{C}^{-1}_{11} = 1/x_1, \tilde{C}^{-1}_{21} = 0, \tilde{C}^{-1}_{31} = 0$.

Because the sum of these elements equals $1/\eta$ (conservation constraint), we have $x_1 = \eta = 0.371$. With $(\tilde{\mathbf{C}}^{-1})_1$ now completely known, we can calculate the spectrum of I_1 from $(\tilde{\mathbf{C}}^{-1})_1$, $\tilde{\mathbf{B}}$, and $\mathbf{A}_p$ using Eq. 3. The result is shown in Fig. 2 *A* (*open squares*). This spectrum of I_1 is in good agreement with that obtained in previous work (25,26).

To calculate the spectrum of the third spectral species, I_2, we proceeded as follows. From Fig. 1 *B*, we note that $\mathbf{B}_1$ reflects a transition between two intermediates with λ_{max} values of ~460 nm (decay of I_1) and 370 nm (rise of I_2). Because there is apparently no contribution from the more blue-shifted species I_2' ($\lambda_{max} \approx 350$ nm) in $\mathbf{B}_1$, which is well known to be formed from I_2 in the next transition (12), I_2' does not contribute to $\tilde{\mathbf{B}}_2$ either. Dye-binding experiments also showed that the formation of the signaling state I_2' is delayed with respect to the formation of I_2 (13). Therefore, we conclude that I_2' is not involved in the first transition, and thus, $z_2 = 0$. The elements x_2, y_2, z_2 of the second column of $\tilde{\mathbf{C}}$ can now be expressed in terms of x_2, y_2, and η with the help of $\tilde{\mathbf{C}}^{-1}\tilde{\mathbf{C}} = \mathbf{I}$. Using the conservation constraint, $x_2 + y_2 = \eta$, we finally obtain for the elements of the second column of $\tilde{\mathbf{C}}^{-1}$, $\tilde{C}^{-1}_{12} = -(\eta - y_2)/\eta y_2, \tilde{C}^{-1}_{22} = 1/y_2, \tilde{C}^{-1}_{32} = 0$. So we have now determined all elements of the second column of $\tilde{\mathbf{C}}^{-1}$, the only free parameter remaining is y_2. Because x_i, y_i, and z_i can assume only positive values and $x_2 + y_2 = \eta$, y_2 is restricted to values between 0 and η. The spectrum of I_2 can now be calculated from $(\tilde{\mathbf{C}}^{-1})_2$, $\tilde{\mathbf{B}}$, and $\mathbf{A}_p$ using Eq. 3. The results are shown in Fig. 2 *B* for six values of y_2 from 0.12 to 0.37 ($\sim\eta$). Because the extinction coefficient has to be positive, physically meaningful absorption spectra are obtained only for $y_2 \geq 0.22$. Of the spectra remaining in Fig. 2 *B*, we pick the one associated with $y_2 = 0.22$ because it has the smallest spectral bandwidth. For y_2 considerably larger than 0.22, the spectral bandwidth becomes much larger than for *P* and I_1, and a secondary absorption maximum develops near 460 nm. This contradicts the original assumption that the UV transitions of I_2 and I_2' are the longest-wavelength transitions of these intermediates, which precludes transitions at higher wavelengths. The spectrum of I_2 for $y_2 = 0.22$ is redrawn in Fig. 2 *A* (*open circles*). Its λ_{max} value is at ~370 ± 5 nm. We note that the value of λ_{max} is independent of the choice of y_2.

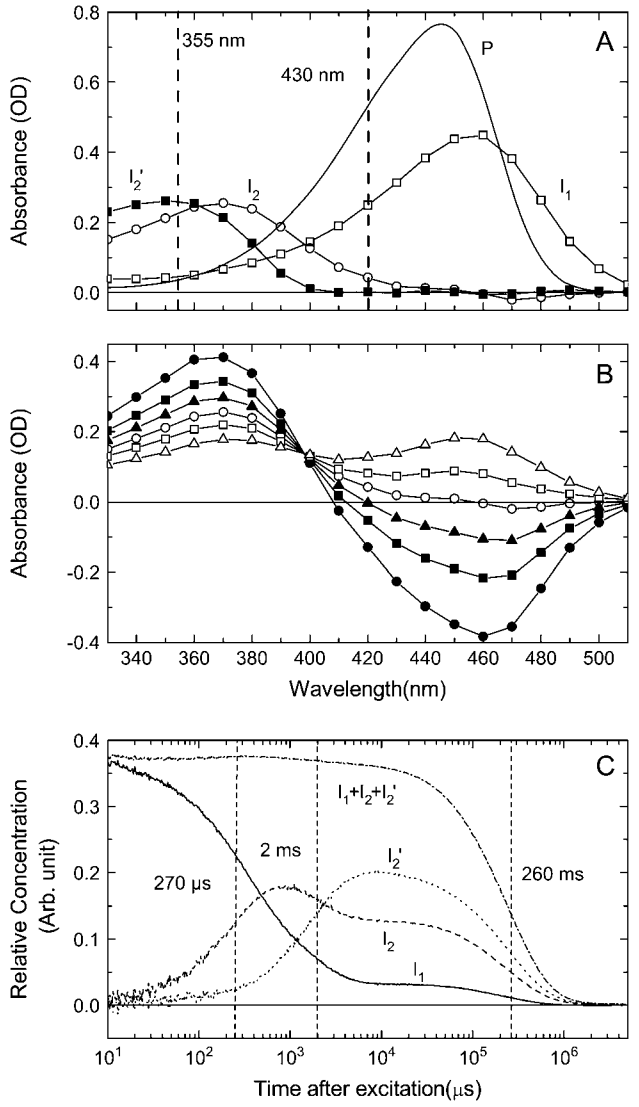

FIGURE 2 (*A*) Intermediate spectra I_1 (□), I_2 (○), and I_2' (■) calculated from the extrapolated difference spectra of Fig. 1 C. The solid curve represents the spectrum of dark state *P* for comparison. Vertical dashed lines indicate the wavelengths of the blue (430 nm) and violet (355 nm) excitation flashes used. (*B*) I_2 spectrum for various allowed values of y_2 as described in the text. $y_2 = 0.12$ (●), $y_2 = 0.15$ (■), $y_2 = 0.18$ (▲), $y_2 = 0.22$ (○), $y_2 = 0.27$ (□), and $y_2 = 0.37$ (Δ). (*C*) Time courses of the relative concentrations of I_1 (*solid line*), I_2 (*dashed line*), and I_2' (*dotted line*) calculated according to Eq. 1. The time course of the sum of the relative concentrations of I_1, I_2, and I_2' is indicated by dashed-dot-dashed line. The vertical dashed lines indicate the time constants from the global SVD fit of Fig. 1 *A*.

With the spectra of I_1, I_2, and I_2', the time courses of the intermediates were calculated from the experimental $\Delta A(\lambda,t)$ data by matrix inversion of Eq. 1. The time dependence of the relative concentrations of the I_1, I_2, and I_2' intermediates at pH 7 are shown in Fig. 2 *C*. I_1 partially decays to I_2 in 270 μs. I_1 and I_2 then further decay around 2 ms to an $I_1/I_2/I_2'$ equilibrium. This equilibrium finally decays to *P* in 260 ms. Also shown is the sum of the relative concentrations of these intermediates (*dash-dot line*). To a good approximation, this sum is constant over the entire time range before the decay to P, validating the data analysis. Its value is very close to $\eta = 0.371$, the fraction cycling, showing the internal consistency of the analysis.

pH dependence of photocycle kinetics

To learn more about the nature of the transition between the acid and the neutral pH regimes, the photocycle kinetics were measured at the following 15 pH values: 4.6, 4.8, 5.1, 5.4, 5.7, 6.0, 6.3, 6.6, 6.75, 6.9, 7.35, 7.7, 7.9, 8.1, 8.4. With excitation at 430 nm, time traces were collected at the seven wavelengths

340, 370, 390, 410, 450, 490, and 500 nm over the time range from 50 ns to 50 s. Results for selected wavelengths are shown in Fig. 3. Note that the panels of Fig. 3 have very different vertical scales and correspondingly different signal/noise ratios. The smallest pH-induced absorbance changes are at 500 nm. The initial absorbance change is almost pH independent at every wavelength, suggesting that the amount of I_1 formed is independent of pH in this range. At each pH, the absorbance changes at all wavelengths could be fitted simultaneously with a sum of three exponentials. The first time constant was virtually constant in this pH range, varying between 200 and 350 μs. The second time constant varied between 1.3 (pH 8.4) and 10.6 (pH 5.1) ms. As we saw above, the first transition results the decay of I_1 to I_2, and the second transition is the decay of I_1/I_2 to the $I_1/I_2/I_2'$ equilibrium. The data of Fig. 3 show that the third time constant, the return of the $I_1/I_2/I_2'$ equilibrium to P, is strongly pH dependent, slowing down with decreasing pH.

Some preliminary conclusions on the pH dependence of the I_1, I_2, I_2' intermediate populations may be drawn by inspection of these data. At 340 nm, the extinction coefficient of I_2' is larger than that of I_2 (Fig. 2 *A*). Although the sequence of time traces is not entirely regular, the absorbance at 340 nm around 10 ms (Fig. 3 *A*) seems to increase with pH, suggesting an increase in the relative amount of I_2'. At 370 nm, the extinction coefficient of I_2 is larger than that of I_2' (Fig. 2 *A*). The decrease in absorbance at 370 nm with pH in the millisecond time range (panel *B* of Fig. 3) may thus be interpreted as a decrease in the relative amount of I_2. At 390 nm, the difference in extinction coefficient between I_2 and I_2' is even larger. This wavelength is therefore diagnostic for the I_2 and I_2' transition and for pH effects on this transition. Panel *C* of Fig. 3 shows the increase in absorbance below 1 ms caused by the I_1-to-I_2 transition (the extinction coefficient of I_2 is larger than that of I_1 at this wavelength, see Fig. 2 *A*). The amount of I_2 formed apparently decreases with increasing pH, judging from the amplitude of the absorption change below 1 ms in Fig. 3 *C*. Around 2–3 ms, there is a large decrease in absorbance caused by the I_2-to-I_2' transition. The amplitude of this transition increases with pH, suggesting that more I_2' is formed at alkaline pH. Panel *D* shows time traces at 410 nm. This wavelength is appropriate for monitoring the I_1' intermediate, which occurs at alkaline pH (25). These traces indicate that this intermediate is absent in this pH range. The traces at 500 nm (panel *F*) are characteristic of I_1. They suggest that, with increasing pH, the I_1-to-I_2 transition slows down somewhat and that more I_1 remains after the I_1/I_2-to-I_2' transition. This is also supported by the traces at 450 nm (panel *E*) indicating that the ground state depletion decreases with pH. In the next section these qualitative conclusions about the pH dependence of the intermediate populations, which were drawn from the data themselves in a model-independent way without any assumptions, are confirmed by a quantitative analysis.

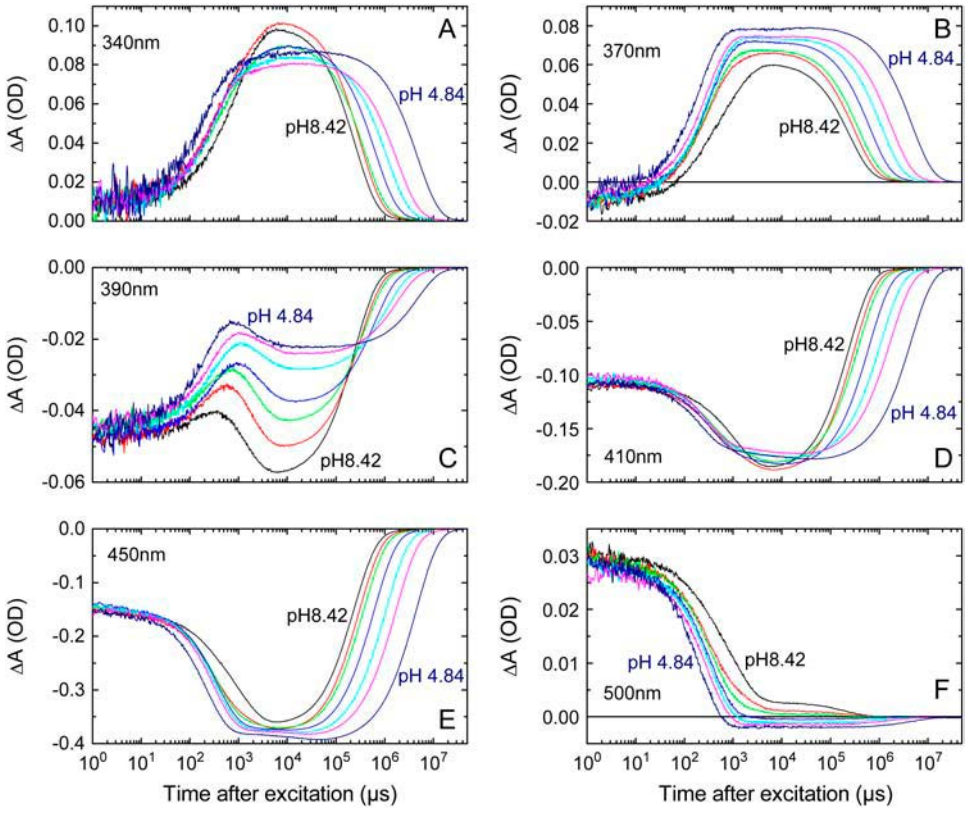

FIGURE 3 pH dependence of the transient absorbance changes after excitation at 430 nm at various wavelengths: (*A*) 340 nm (characteristic for I_2'), (*B*) 370 nm (characteristic for I_2), (*C*) 390 nm (characteristic for I_2), (*D*) 410 nm (characteristic for I_1'), (*E*) 450 nm (characteristic for P), and (*F*) 500 nm (characteristic for I_1). The color codes for the pH values in each panel are the following: black, pH 8.4; red, pH 6.9; green, pH 6.6; blue, pH 6.0; light blue, pH 5.7; pink, pH 5.4; dark blue, pH 4.8. Conditions: 50 mM MES, 50 mM KCl, 20°C. PYP concentration 53 μM.

To obtain the time courses of the intermediate populations, it was assumed that the spectra of I_1, I_2, and I_2' of Fig. 2 *A* are pH independent and that no other intermediates contribute in the pH range from 4.6 to 8.4. Equation 1 was then used to calculate the time traces $n_i(t)$ for each intermediate at each pH value from the absorbance changes $\Delta A(\lambda, t)$ and the spectra $A_i(\lambda)$ by matrix inversion. The time dependencies of the populations of I_1, I_2, and I_2' at 7 of the 15 pH values are shown in panels *A*, *B*, and *C* of Fig. 4. They confirm what was suggested by the data of Fig. 3: I_1 decays partially to I_2; I_2 then partially decays to I_2'; beyond 10 ms I_1, I_2, and I_2' are in equilibrium and return together to P. Fig. 4 *D* shows that the sum of the populations is approximately constant in time and equal to the fraction cycling. Whereas the population of I_1 in equilibrium with I_2 and I_2' is only slightly pH dependent (see traces in Fig. 4 *A* around 10 ms), the concentrations of I_2 and I_2' show a strong and opposite pH dependence. With increasing pH, the amount of I_2' increases at the expense of a corresponding decrease in the I_2 population. To quantify this pH dependence of the equilibrium populations, their concentrations at 10 ms were taken from Fig. 4, *B* and *C* (*vertical dashed lines*). The corresponding concentrations of I_2 and I_2' are plotted in Fig. 5 *A* as a function of pH. The solid curves are the results of a simultaneous fit with the Henderson-Hasselbalch equation. The fit parameters were $pK_a \approx 6.4$ and $n \approx 0.98$. I_2 and I_2' are thus in a pH-dependent equilibrium.

The ground state recovery slows down at acid pH. The rate constant k_3 for this recovery was determined from a global fit of the data of Fig. 3 at all seven wavelengths. Its pH dependence is plotted in Fig. 5 *B*. A fit with the Henderson-Hasselbalch equation results in a pK_a of ~6.3 and n of ~0.8 . The apparent decay rate for the dark-state recovery thus seems to be proportional to the I_2' population in the $I_1/I_2/I_2'$ equilibrium. This relationship is expected in the framework of a simple model presented in the discussion.

pH dependence of photoreversal kinetics

Recently, we measured and analyzed the kinetics of photoreversal from I_2, I_2', and I_1 at pH 6 in detail (33). The time delay between the two flashes was varied from 1 μs to 3 s, and the photoreversal kinetics were measured at 26 wavelengths from 330 to 510 nm (33). The photoreversal time traces at pH 6 required two exponentials for an adequate fit with well-separated time constants of $\tau_1 = 60$ and $\tau_2 = 400$ μs. These time constants were assigned to photoreversal from I_2 (60 μs) and I_2' (400 μs), respectively, on the basis of the delay dependence of the amplitudes (33). Moreover, we found that I_2 and I_2' are in equilibrium (33). Here, our focus is on the pH dependence. The photoreversal kinetics were therefore measured at only two wavelengths (340 and 450 nm) and at the fixed delay of 20 ms. At this time delay all three intermediates I_2, I_2', and I_1 are present and in equilibrium (Figs. 2 *C* and 4).

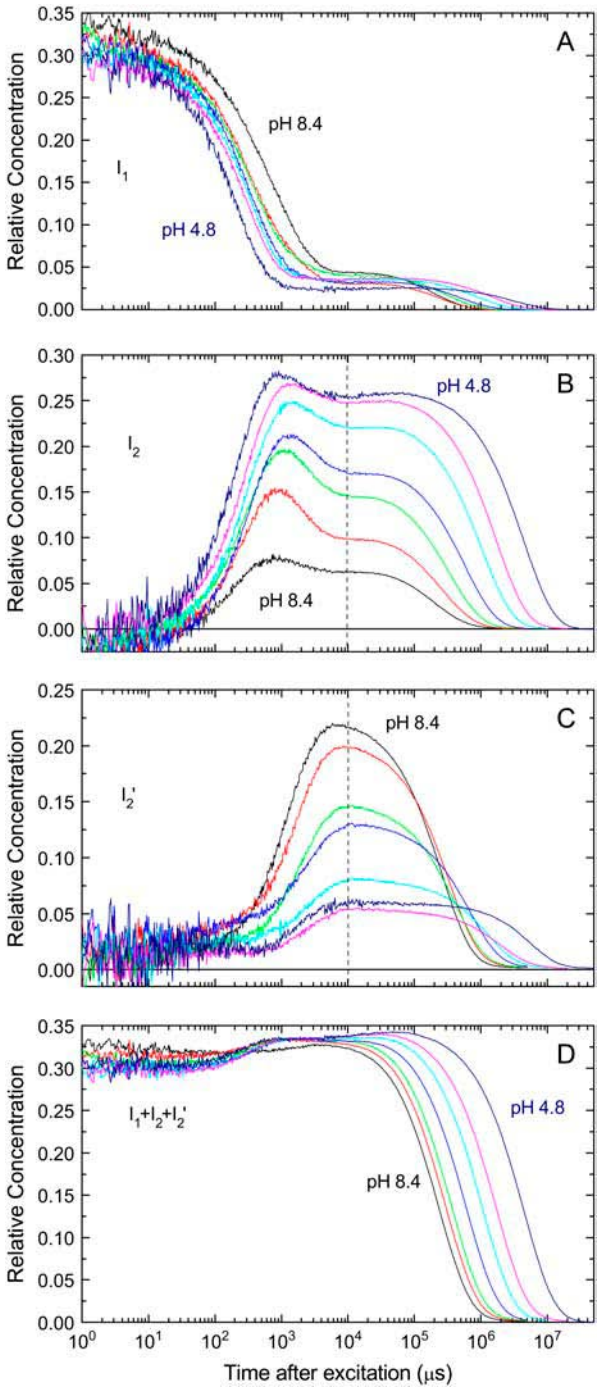

FIGURE 4 Time courses of the relative concentrations of the I_1 (*A*), I_2 (*B*), and I_2' (*C*) intermediates at various pH values calculated using Eq. 1 as explained in the text. (*D*) Time course of the sum of the populations of I_1, I_2, and I_2'. Color code as in Fig. 3.

The photoreversal signals at pH 5.1 and 8.1 are shown in Fig. 6 *A*. For clarity, only the traces at 2 of the 15 pH values are shown together with their simultaneous fits (*solid lines*). As at pH 6 (33), the kinetics required two exponentials over the pH range from 4.6 to 6.9. These two phases can be clearly discerned in the data at pH 5.1. From pH 7.3 on, only the

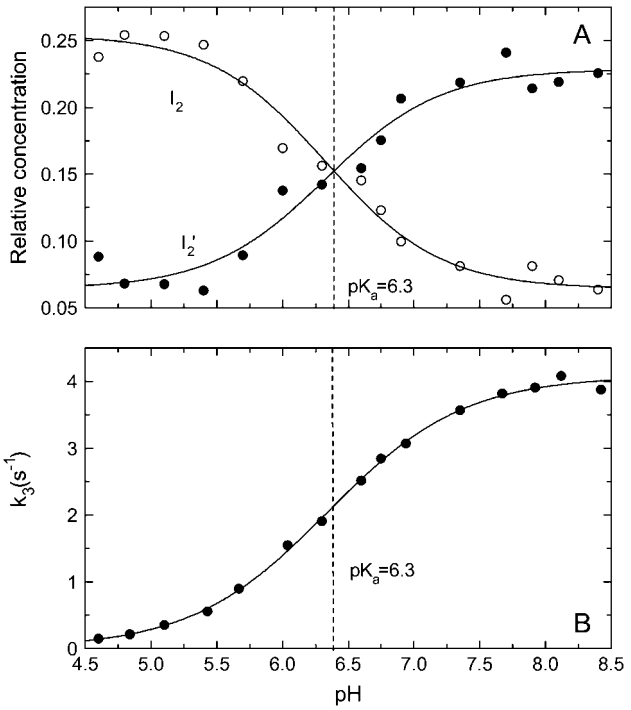

FIGURE 5 (*A*) pH dependence of the equilibrium concentrations of the I_2 (○) and I_2' (●) intermediates at 10 ms derived from Fig. 4, *B* and *C*, respectively. The solid curves are simultaneous fits of these titration curves with the Henderson-Hasselbalch equation with $pK_a = 6.4$ and $n \approx 0.98$. (*B*) pH dependence of the decay rate k_3 of the ground-state recovery. For every pH, the decay rate k_3 was derived from the simultaneous fit of the measured transient absorbance changes at 340 nm, 370 nm, 390 nm, 410 nm, 450 nm, 490 nm, and 500 nm with a sum of three exponentials. The solid curve in *B* is the fit of the decay rate k_3 with the Henderson-Hasselbalch equation with $pK_a = 6.3$, $n \approx 0.84$.

slow component was required. The fast time constant was virtually pH independent, varying between 48 and 63 μs. The second time constant varied between 330 and 770 μs in the pH range investigated. Comparison of the time traces in Fig. 6 *A* makes it clear that there are significant differences between pH 5.1 and 8.1. The total initial photoreversal signal is somewhat larger at pH 5.1 than at 8.1, suggesting that more I_2/I_2' can be photoreversed. The amplitude data provide further insight. The pH dependence of the amplitudes A_1 and A_2 (for the corresponding time constants τ_1 and τ_2) are plotted in Fig. 6, *B* (340 nm) and *C* (450 nm). These figures confirm that, with increasing pH, A_1 becomes smaller, approaching zero around pH 7 at both wavelengths, whereas A_2 shows a corresponding increase. The solid curves are simultaneous fits of the amplitudes at 340 and 450 nm with the Henderson-Hasselbalch equation, with $pK_a = 6.1$ and $n = 1.9$. We assigned A_1 and A_2 to photoreversal from I_2 and I_2', respectively (33). The results of Fig. 6, *B* and *C* thus suggest that, with increasing pH, the I_2/I_2' equilibrium shifts from I_2 at pH 4.6 to I_2' at pH 8.4. These results, from the pH dependence of the photoreversal amplitudes, thus support our observations from the photocycle, where a pK_a of 6.4 was obtained. We note that in the photocycle experiments, $n = 0.98$ (I_2/I_2' equilibrium) or 0.8 (recovery rate), whereas we obtained $n = 1.9$ from the photoreversal kinetics. The photoreversal absorbance changes required various corrections and are, moreover, quite small. The errors are correspondingly large. The photocycle data points, on the other hand, display much less scattering, in particular for k_3, and did

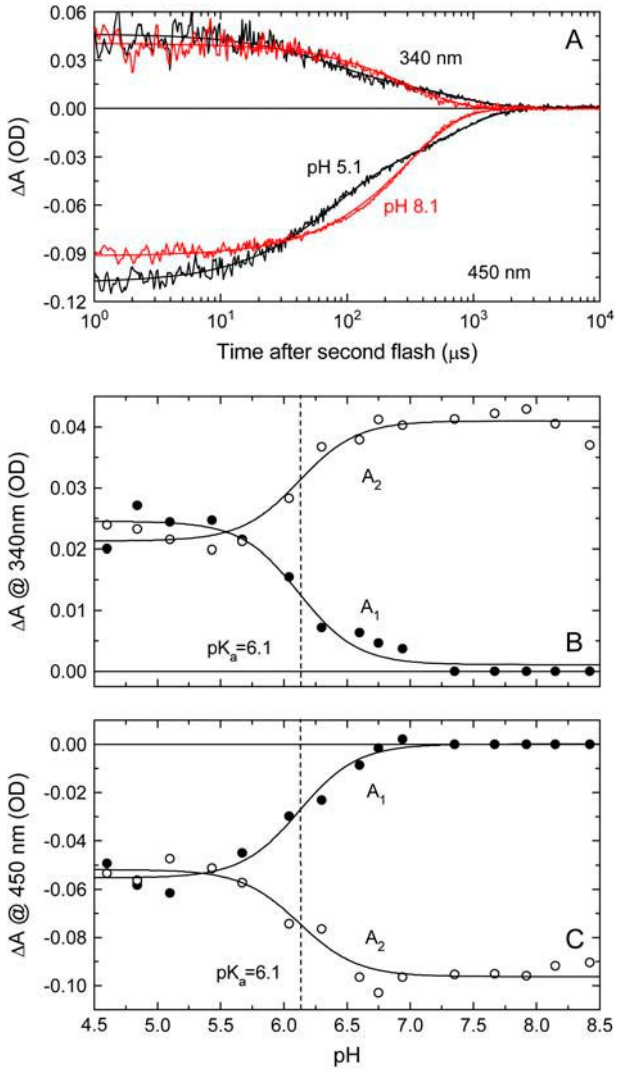

FIGURE 6 (*A*) Photoreversal signals, at 340 nm (*positive*) and 450 nm (*negative*) at pH 5.1 (*black*) and 8.1 (*red*), calculated as described in the text. For clarity, the data obtained at 13 other pH values ranging from 4.6 to 8.4 are not shown. The solid curves represent a simultaneous exponential fit to the 340-nm and 450-nm traces. Conditions: 20°C, 50 mM KCl and 50 mM MES, PYP concentration 53 μM. The delay between first (*blue,* 430 nm) and second (*violet,* 355 nm) flashes is 20 ms. (*B* and *C*) pH dependence of the photoreversal amplitudes A_1 and A_2 at 340 nm (*B*) and 450 nm (*C*). A_1 (●) and A_2 (○) are the amplitudes of the fast (48–60 μs) and slow (300–770 μs) components, respectively, obtained from the simultaneous fit of the 340-nm and 450-nm traces of panel *A*. The solid curves of panels *B* and *C* represent a common fit to the pH dependence of all four amplitudes with the Henderson-Hasselbalch equation, with a pK_a of 6.1 (*dashed vertical lines*) and a Hill coefficient of 1.9.

not require complex corrections. We believe, therefore, that the number of protons involved is one in both experiments.

DISCUSSION

From measurements of the pH dependence of the photocycle and photoreversal kinetics of PYP between 4.6 and 8.4, we obtained the following results: 1) the spectra of the signaling state I_2' (350 nm) and its precursor I_2 (370 nm) differ by ~20 nm; 2) from several milliseconds (formation of I_2') to the end of the cycle, the three intermediates I_1, I_2, and I_2' are in equilibrium; and 3) the pK_a of the pH-dependent equilibrium between I_2' and its precursor I_2 is ~6.4 from photocycle kinetics and ~6.1 from photoreversal kinetics. The pH is thus an important parameter that controls the amount of receptor in the active state. This is analogous to the case of the photoreceptor rhodopsin, where the equilibrium between the signaling state M_{II} and its precursor M_I is also strongly pH dependent (e.g., (43)). We recently showed (26) that the I_2/I_2' equilibrium, like the M_I/M_{II} equilibrium (44), also depends on the salt concentration. In both photoreceptors, high salt favors the signaling state. The proposed reaction scheme for the kinetics and equilibria of the photocycle in this pH range is presented in Fig. 7.

The existence of two distinguishable I_2 intermediates with protonated chromophores was first demonstrated by time-resolved FTIR (12,18). I_2 decays to I_2' in ~2–3 ms (12,18). This transition to the signaling state I_2' is characterized by a global conformational change (12,18). Here, we showed that this transition may also be monitored by transient electronic absorption spectroscopy and determined the absorption

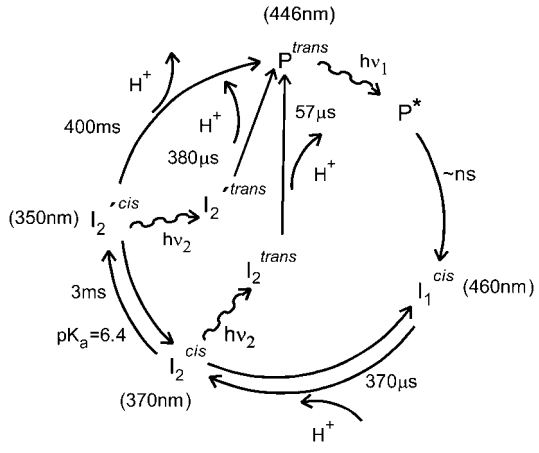

FIGURE 7 Proposed model for the kinetics of the photocycle and photoreversal of PYP in the pH range from 4 to 8. The I_2^{cis} and $I_2'^{cis}$ intermediates are in a pH-dependent equilibrium and photoreverse to P^{trans} with exponential time constants of 57 and 380 μs. The pK_a of the $I_2^{cis}/I_2'^{cis}$ equilibrium is 6.4. Note the equilibria among I_1, I_2, and I_2'. These three intermediates decay together to P. For clarity the short-lived intermediates I_0 and $I_0^{\ddagger}$ between P* and I_1 are not shown. The proton arrows indicate the transient uptake and release of protons as detected by a pH-sensitive dye in solution (13).

spectra of I_2 and I_2' by the extrapolated difference method (25,37). The λ_{max} values of I_2 and I_2' are 370 ± 5 and 350 ± 5 nm, respectively. Absorption spectra for I_2 and I_2' at pH 8.1 were presented by Hendriks et al. (11). No λ_{max} values were provided, but the spectrum of I_2 was said to be ''slightly red-shifted'' with respect to I_2' in agreement with our results. The spectrum of I_2 presented by Hendriks et al. (11) is so noisy that it is difficult to estimate λ_{max}. The poor quality of this spectrum is probably caused by the fact that at pH 8.1 the contribution of I_2 in the equilibrium is very low, as we showed here (Fig. 5 *A*).

Using the spectra of I_2 and I_2' from Fig. 2 *A* and assuming that they are pH independent in the pH range from 4.6 to 8.4, we obtained the time dependence of the concentrations of I_1, I_2, and I_2' (Fig. 4). From ~5 ms onward, I_1, I_2, and I_2' are in equilibrium and decay together to the initial dark state P. The equilibrium intermediate populations of I_2 and I_2' are pH dependent with a pK_a of ~6.4. Below the pK_a, I_2 is the major species; above the pK_a the opposite holds. We note that these transitions are not complete (Fig. 5 *A*).

The sum of the populations of the I_1, I_2, and I_2' intermediates in Fig. 4 *D* is not as constant in time for every pH as it should be and as it is at pH 7 (Fig. 2 *C*). One cause could be that the intermediate spectra are not exactly pH independent over the whole pH range, so that the spectra derived at pH 7 are not quite correct for every pH. So we derived a second set of intermediate spectra from a joint SVD analysis over the whole pH range as in Joshi et al. (25). These are the best pH-averaged intermediate spectra. The differences with the set at pH 7 (Fig. 2 *A*) are small. A third set was obtained from the scaled subtraction method (25). All three sets of intermediate spectra lead to the same pK_a value. The results differed only somewhat in terms of the end values of the titrations at high pH. The sum of the populations remained slightly time-dependent, however, and other inadequacies developed, such as slightly negative populations. Because the spectra of I_2 and I_2' are quite similar, the analysis is sensitive to the small differences between them. We believe this is the likely source of the error in Fig. 4 *D*.

Measurements of the pH dependence of the photoreversal kinetics of I_2 and I_2' at a delay of 20 ms (Fig. 6) provide further support for this pK_a. The kinetics are characterized by a fast (50–60 μs) and a slow (300–800 μs) component, which result from photoreversal from I_2 and I_2', respectively (33). The corresponding amplitudes are pH dependent (Fig. 6, *B* and *C*) with a pK_a of 6.1, in good agreement with the value of 6.4 obtained from the photocycle kinetics. The amplitude for I_2 goes to zero beyond pH 7.3. The photoreversal data thus suggest that no I_2 remains at alkaline pH, whereas the photocycle data indicate that some I_2 remains because $[I_2]/([I_2] + [I_2'])$ is ~0.25 at pH 8.6 (Fig. 5 *A*). We note that the end value of the I_2 population at high pH in Fig. 5 *A* is quite sensitive to the exact choice of the I_1 spectrum. In a recent investigation on the intermediates and spectra at alkaline pH (25), we found that only three intermediates, I_1, I_1', and I_2', are present above pH 8, i.e., no I_2.

The pH dependence of the absorption spectrum of a photostationary mixture of P, I_2, and I_2' produced by background illumination was recently analyzed by SVD (34). It was shown that I_2 and I_2' are in a pH-dependent equilibrium with a pK_a of 6.3 and that the spectrum of the high-pH species I_2' is blue-shifted with respect to that of the low-pH species I_2 (34). The I_2 and I_2' intermediates also differ with regard to the fluorescence lifetime of the single tryptophan of PYP, W-119 (34). In I_2, the lifetime is long (0.82 ns). In I_2', the lifetime is much shorter (0.04 ns). Using background illumination, these authors showed that the fluorescence decay in the photostationary state is pH dependent with I_2 dominating at low pH and I_2' at high pH (34). The pK_a was ~6.3. Combining the pH dependence of the fluorescence amplitudes with that of the photostationary absorption, absorption spectra were calculated for the I_2 and I_2' species. These had λ_{max} values of 372 and 352 nm for I_2 and I_2', respectively (34), in good agreement with the results reported in this work.

The results on the pH dependence of the I_2/I_2' equilibrium (34) were recently confirmed (29). Analysis of the photostationary absorption spectra by a scaled subtraction procedure yielded a pK_a of 6.4 and λ_{max} values of 367 and 356 nm for I_2 and I_2', respectively (29). These authors showed, moreover, from CD and small-angle x-ray scattering experiments that the global structural transition occurs between these two intermediates with a pK_a of 6.4. Together with the kinetics results from time-resolved absorption spectroscopy presented here, these complementary methods lead to a comprehensive picture of the I_2-to-I_2' equilibrium.

As is well known (23) and confirmed here (Fig. 5 *C*), the rate k_3, for the ground state recovery, is also pH dependent with a pK_a of 6.3, i.e., within experimental error equal to that for the I_2/I_2' equilibrium (6.4 and 6.1, from single flash photolysis and photoreversal measurements, respectively). Thus, k_3 seems to be proportional to the I_2' population (compare Fig. 5, *A* and *B*). Such a proportionality is expected under the following conditions: 1) the equilibration rates among I_1, I_2, and I_2' are rapid compared to the microscopic rates of return from each intermediate to the ground state; 2) the latter are pH independent; and 3) the rate from I_2' to P is much larger than from the other intermediates. A similar model was recently proposed to explain the pH dependence of the rate of ground state recovery at alkaline pH (25). At alkaline pH, the I_1, I_1', and I_2' intermediates are in equilibrium. The pK_a of the I_1'-to-I_2' equilibrium is ~9.9, and the ground state recovery rate constant k_3 has a pK_a of 9.7 and is proportional to the I_2' population. There is thus a striking similarity between the behavior at high and low pH. For both branches of the bell-shaped pH dependence of k_3, it seems that k_3 is proportional to $[I_2']$. This proportionality is not exact however, because k_3 approaches zero at low pH, whereas $[I_2']$ approaches a constant value unequal to zero. A more detailed model thus seems to be required. Nevertheless, this symmetry between low and high pH behavior is worth pointing out, and the underlying model provides a lowest-order explanation.

An important question concerns the group responsible for the pK_a of ~6.4. The similar pK_a for the recovery rate k_3 is commonly attributed to the carboxyl group of E-46 (35,36). We now need to discuss this pK_a in the context of the underlying I_2/I_2' equilibrium. What is the mechanism whereby a change in protonation of E-46 shifts the equilibrium from I_2 to I_2'. In I_2 the chromophore is already protonated and has moved away from E-46 toward the surface (6). If E-46 is the internal proton donor for the chromophore, its carboxyl group is presumably already deprotonated in I_2, in accordance with some observations from time-resolved FTIR (12). In I_2' the chromophore remains protonated, but the protein structure is changed in a major way. It is unclear how the deprotonated E-46 could affect the I_2/I_2' conformational equilibrium. If, however, E-46 is not the internal proton donor, and the chromophore is protonated from the external medium, as suggested (13), E-46 could remain protonated in I_2 and be deprotonated in I_2'. In other time-resolved FTIR measurements (18), a positive band was observed at 1759 cm^{-1} with a risetime of 113 μs (formation of I_2) and assigned to an environmental shift of the protonated E-46. Brudler et al. (18) were not aware of the I_2/I_2' equilibrium and concluded from the fact that the amplitude of the positive band was significantly smaller than that of the negative band due to the initial dark state, that only a fraction of the molecules cycling had a protonated E-46 in I_2. Their experiments were, however, performed in buffer at pH 7. At this pH, the I_2/I_2' equilibrium is far on the side of I_2' (see Fig. 5 *A*), so that only a minority of molecules would have been in the I_2 state. It is thus consistent with the time-resolved data of (18) to conclude that in I_2 the carboxyl group of E-46 is protonated. Recent photostationary FTIR measurements also indicate that E-46 is at least partially protonated in I_2 (29). A role of E-46 in controlling the I_2/I_2' equilibrium is thus plausible. In the absence of the carboxyl group, in the mutant E46Q, the conformational change in I_2' is much smaller or absent (12), and the absorption maximum at pH 7 is at 368 nm (45), i.e., I_2-like. These results suggest that in the absence of E-46 the I_2/I_2' equilibrium is predominantly or entirely on the side of I_2 and further support the idea that E-46 is responsible for the wild-type pK_a of 6.4. We note that this reinterpretation of the FTIR results is consistent with a mechanism of chromophore protonation from the external medium (13).

Another residue that might be involved is H-108. The pH dependence of the steady-state proton uptake was investigated (46), and from the observed pH dependence, a pK_a of 6.6 was obtained, which was attributed to histidine-108. This residue is located on the central β-scaffold and may be involved in the interaction between the β-scaffold and the N-terminal domain. It was recently postulated, on the basis of the observation that the I_2-to-I_2' transition is blocked at low salt concentrations, that the loss of this interaction is a prerequisite for the formation of I_2' (26).

Recently two forms of I_1 could be distinguished on the basis of their resonance Raman spectra, which are in a

pH-dependent equilibrium with a pK_a of ~6.2 (30). The low-pH form (I_1^{ℓ}) lacks the hydrogen bond with E-46, whereas the high-pH form (I_1^{h}) has both hydrogen bonds. It is possible that the pH dependence observed here for the I_2/I_2' equilibrium results from the pH dependence of the preceding I_1^{ℓ}/I_1^{h} equilibrium.

In conclusion, we have shown from measurements of the time-dependent intermediate populations that the equilibrium between I_2 and I_2' and the formation of the signaling state I_2' are pH dependent with a pK_a of ~6.4. The intracellular pH may thus regulate the amount of active receptor. The value of this pK_a provides an explanation for the similar well-known pK_a of the rate constant for the ground-state recovery. We find, moreover, that I_2' is blue-shifted with respect to I_2 by ~20 nm, suggesting a different chromophore environment for the exposed chromophore in the signaling state.

This work was supported by the National Institutes of Health (grant GM 66146 to M.A.C.) and the Deutsche Forschungsgemeinschaft (grant GK 788 TP A9 to M.P.H.).

REFERENCES

1. Cusanovich, M. A., and T. E. Meyer. 2003. Photoactive yellow protein: a prototypic PAS domain sensory protein and development of a common signaling mechanism. *Biochemistry.* 42:4759–4770.
2. Taylor, B. L., and I. B. Zhulin. 1999. PAS domains: internal sensors of oxygen, redox potential, and light. *Microbiol. Mol. Biol. Rev.* 63: 479–506.
3. Borgstahl, G. E. O., D. R. Williams, and E. D. Getzoff. 1995. 1.4 Å structure of photoactive yellow protein, a cytosolic photoreceptor: unusual fold, active site and chromophore. *Biochemistry.* 34:6278–6287.
4. Rajagopal, S., S. Anderson, V. Srajer, M. Schmidt, R. Pahl, and K. Moffat. 2005. A structural pathway for signalling in the E46Q mutant of photoactive yellow protein. *Structure.* 13:55–63.
5. Ihee, H., S. Rajagopal, V. Šrajer, R. Pahl, S. Anderson, M. Schmidt, F. Schotte, P. A. Anfinrud, M. Wulff, and K. Moffat. 2005. Visualizing reaction pathways in photoactive yellow protein from nanoseconds to seconds. *Proc. Natl. Acad. Sci. USA.* 102:7145–7150.
6. Genick, U. K., G. E. Borgstahl, K. Ng, Z. Ren, C. Pradervand, P. M. Burke, V. Srajer, T. Y. Teng, W. Schildkamp, D. E. McRee, K. Moffat, and E. D. Getzoff. 1997. Structure of a protein photocycle intermediate by millisecond time-resolved crystallography. *Science.* 275:1471–1475.
7. Dux, P., G. Rubinstenn, G. W. Vuister, R. Boelens, F. A. A. Mulder, K. Hard, W. D. Hoff, A. R. Kroon, W. Crielaard, K. J. Hellingwerf, and R. Kaptein. 1998. Solution structure and backbone dynamics of the photoactive yellow protein. *Biochemistry.* 37:12689–12699.
8. Sprenger, W. W., W. D. Hoff, J. P. Armitage, and K. J. Hellingwerf. 1993. The eubacterium *Ectothiorhodospira halophila* is negatively phototactic, with a wavelength dependence that fits the absorption spectrum of photoactive yellow protein. *J. Bacteriol.* 175:3096–3104.
9. Hoff, W. D., I. H. M. van Stokkum, H.-J. van Ramesdonk, M. E. van Brederode, A. M. Brouwer, J. C. Fitch, T. E. Meyer, R. van Grondelle, and K. J. Hellingwerf. 1994. Measurement and global analysis of the absorbance changes in the photocycle of the photoactive yellow protein from *Ectothiorhodospira halophila*. *Biophys. J.* 67:1691–1705.
10. Ujj, L., S. Devanathan, T. E. Meyer, M. A. Cusanovich, G. Tollin, and G. H. Atkinson. 1998. New photocycle intermediate in the photoactive yellow protein from *Ectorhodospira halophila:* picosecond transient absorption spectroscopy. *Biophys. J.* 75:406–412.
11. Hendriks, J., I. H. M. van Stokkum, and K. J. Hellingwerf. 2003. Deuterium isotope effects in the photocycle transitions of the photoactive yellow protein. *Biophys. J.* 84:1180–1191.
12. Xie, A., L. Kelemen, J. Hendriks, B. J. White, K. J. Hellingwerf, and W. D. Hoff. 2001. Formation of a new buried charge drives a large-amplitude protein quake in photoreceptor activation. *Biochemistry.* 40:1510–1517.
13. Borucki, B., S. Devanathan, H. Otto, M. A. Cusanovich, G. Tollin, and M. P. Heyn. 2002. Kinetics of proton uptake and dye binding by photoactive yellow protein in wildtype and in the E46Q and E46A mutants. *Biochemistry.* 41:10026–10037.
14. Rubinstenn, G., G. W. Vuister, F. A. A. Mulder, P. E. Dux, R. Boelens, K. J. Hellingwerf, and R. Kaptein. 1998. Structural and dynamic changes of photoactive yellow protein during its photocycle in solution. *Nat. Struct. Biol.* 5:568–570.
15. Bernhard, C., K. Houben, N. M. Derix, D. Marks, M. A. van der Horst, K. J. Hellingwerf, R. Boelens, R. Kaptein, and N. A. J. van Nuland. 2005. The solution structure of a transient photoreceptor intermediate: Δ25 photoactive yellow protein. *Structure.* 13:953–962.
16. Lee, B.-C., P. A. Croonquist, T. R. Sosnick, and W. D. Hoff. 2001. PAS domain receptor photoactive yellow protein is converted to a molten globule state upon activation. *J. Biol. Chem.* 276:20821–20823.
17. Imamoto, Y., H. Kamikubo, M. Harigai, N. Shimizu, and M. Kataoka. 2002. Light-induced global conformational change of photoactive yellow protein in solution. *Biochemistry.* 41:13595–13601.
18. Brudler, R., R. Rammelsberg, T. T. Woo, E. D. Getzoff, and K. Gerwert. 2001. Structure of the I_1 early intermediate of photoactive yellow protein by FTIR spectroscopy. *Nat. Struct. Biol.* 8:265–270.
19. Meyer, T. E., G. Tollin, J. H. Hazzard, and M. A. Cusanovich. 1989. Photoactive yellow protein from the purple phototropic bacterium, *Ectothiorhodospira halophila*: quantum yield of photobleaching and effects of temperature, alcohols, glycerol, and sucrose on kinetics of photobleaching and recovery. *Biophys. J.* 56:559–564.
20. Meyer, T. E., E. Yakali, M. A. Cusanovich, and G. Tollin. 1987. Properties of a water-soluble, yellow protein isolated from a halophilic phototrophic bacterium that has photochemical activity analogous to sensory rhodopsin. *Biochemistry.* 26:418–423.
21. Unno, M., M. Kumauchi, J. Sasaki, F. Tokunaga, and S. Yamauchi. 2000. Evidence for a protonated and *cis* configuration chromophore in the photobleached intermediate of photoactive yellow protein. *J. Am. Chem. Soc.* 122:4233–4234.
22. Pan, D., A. Philip, W. D. Hoff, and R. A. Mathies. 2004. Time-resolved resonance Raman structural studies of the pB' intermediate in the photocycle of photoactive yellow protein. *Biophys. J.* 86:2374–2382.
23. Genick, U. K., S. Devanathan, T. E. Meyer, I. L. Canestrelli, E. Williams, M. A. Cusanovich, G. Tollin, and E. D. Getzoff. 1997. Active site mutants implicate key residues for control of color and light cycle kinetics of photoactive yellow protein. *Biochemistry.* 36: 8–14.
24. Borucki, B., H. Otto, C. P. Joshi, C. Gasperi, M. A. Cusanovich, S. Devanathan, G. Tollin, and M. P. Heyn. 2003. pH dependence of the photocycle kinetics of the E46Q mutant of photoactive yellow protein: protonation equilibrium between the I_1 and I_2 intermediates, chromophore deprotonation by hydroxyl uptake, and protonation relaxation in the dark state. *Biochemistry.* 42:8780–8790.
25. Joshi, C. P., B. Borucki, H. Otto, T. E. Meyer, M. A. Cusanovich, and M. P. Heyn. 2006. Photocycle and photoreversal of photoactive yellow protein at alkaline pH: kinetics, intermediates and equilibria. *Biochemistry.* 45:7057–7068.
26. Borucki, B., J. A. Kyndt, C. P. Joshi, H. Otto, T. E. Meyer, M. A. Cusanovich, and M. P. Heyn. 2005. Effect of salt and pH on the activation of photoactive yellow protein and gateway mutants Y98Q and Y98F. *Biochemistry.* 44:13650–13663.
27. Harigai, M., Y. Imamoto, H. Kamikubo, Y. Yamazaki, and M. Kataoka. 2003. Role of an N-terminal loop in the secondary structural change of photoactive yellow protein. *Biochemistry.* 42:13893–13900.

28. Imamoto, Y., M. Harigai, and M. Kataoka. 2004. Direct observation of the pH-dependent equilibrium between L-like and M intermediates of photoactive yellow protein. *FEBS Lett.* 577:75–80.

29. Shimizu, N., Y. Imamoto, M. Harigai, H. Kamikubo, Y. Yamazaki, and M. Kataoka. 2006. pH-dependent equilibrium between long lived near-UV intermediates of photoactive yellow protein. *J. Biol. Chem.* 281:4318–4325.

30. Unno, M., M. Kumauchi, N. Hamada, F. Tokunaga, and S. Yamauchi. 2004. Resonance Raman evidence for two conformations involved in the L intermediate of photoactive yellow protein. *J. Biol. Chem.* 279: 23855–23858.

31. Miller, A., H. Leigeber, W. D. Hoff, and K. J. Hellingwerf. 1993. A light-dependent branching reaction in the photocycle of the yellow protein from *Ectothiorhodospira halophila*. *Biochim. Biophys. Acta.* 1141:190–196.

32. Hendriks, J., I. H. M. van Stokkum, W. Crielaard, and K. J. Hellingwerf. 1999. Kinetics of and intermediates in a photocycle branching reaction of the photoactive yellow protein from *Ectothiorhodospira halophila*. *FEBS Lett.* 458:252–256.

33. Joshi, C. P., B. Borucki, H. Otto, T. E. Meyer, M. A. Cusanovich, and M. P. Heyn. 2005. Photoreversal kinetics of the I_1 and I_2 intermediates in the photocycle of photoactive yellow protein by double flash experiments with variable time delay. *Biochemistry.* 44:656–665.

34. Otto, H., D. Hoersch, T. E. Meyer, M. A. Cusanovich, and M. P. Heyn. 2005. Time-resolved single tryptophan fluorescence in photoactive yellow protein monitors changes in the chromophore structure during the photocycle via energy transfer. *Biochemistry.* 44:16804–16816.

35. Meyer, T. E., S. Devanathan, T. Woo, E. D. Getzoff, G. Tollin, and M. A. Cusanovich. 2003. Site-specific mutations provide new insights into the origin of pH effects and alternative spectral forms in the photoactive yellow protein from *Halorhodospira halophila*. *Biochemistry.* 42:3319–3325.

36. Demchuk, E., U. K. Genick, T. T. Woo, E. D. Getzoff, and D. Bashford. 2000. Protonation states and pH titration of the photocycle of photoactive yellow protein. *Biochemistry.* 39:1100–1113.

37. Borucki, B., H. Otto, and M. P. Heyn. 1999. Reorientation of the retinylidene chromophore in the K, L, and M intermediates of bacteriorhodopsin from time-resolved linear dichroism: resolving kinetically and spectrally overlapping intermediates of chromoproteins. *J. Phys. Chem. B.* 103:6371–6383.

38. Kyndt, J. A., F. Vanrobaeys, J. C. Fitch, B. V. Devreese, T. E. Meyer, M. A. Cusanovich, and J. J. Van Beeumen. 2003. Heterologous production of *Halorhodospira halophila* holo-photoactive yellow protein through tandem expression of the postulated biosynthetic genes. *Biochemistry.* 42:965–970.

39. Dickopf, S., and M. P. Heyn. 1997. Evidence for the first phase of the reprotonation switch of bacteriorhodopsin from time-resolved photovoltage and flash photolysis experiments on the photoreversal of the M-intermediate. *Biophys. J.* 73:3171–3181.

40. Hendler, R. W., and R. I. Shrager. 1994. Deconvolutions based on singular value decomposition and pseudo inverse: a guide for beginners. *J. Biochem. Biophys. Methods.* 78:1–33.

41. Henry, E. R., and J. Hofrichter. 1992. Singular value decomposition: application to analysis of experimental data. *Methods Enzymol.* 210: 129–192.

42. Borucki, B., H. Otto, G. Rottwinkel, J. Hughes, M. P. Heyn, and T. Lamparter. 2003. Mechanism of Cph1 phytochrome assembly from stopped-flow kinetics and circular dichroism. *Biochemistry.* 42:13684–13697.

43. Dickopf, S., T. Mielke, and M. P. Heyn. 1998. Kinetics of the light-induced proton translocation associated with the pH-dependent formation of the metarhodopsin I/II equilibrium of bovine rhodopsin. *Biochemistry.* 37:16888–16897.

44. Vogel, R., and F. Siebert. 2002. Conformation and stability of α-helical membrane proteins. 1. Influence of salts on conformational equilibria between active and inactive states of rhodopsin. *Biochemistry.* 41: 3529–3535.

45. Imamoto, Y., K. Mihara, F. Tokunaga, and M. Kataoka. 2001. Spectroscopic characterization of the photocycle intermediates of photoactive yellow protein. *Biochemistry.* 40:14336–14343.

46. Hendriks, J., W. D. Hoff, W. Crielaard, and K. J. Hellingwerf. 1999. Protonation deprotonation reactions triggered by photoactivation of photoactive yellow protein from *Ectothiorhodospira halophila*. *J. Biol. Chem.* 274:17655–17660.